THE JOURNAL OF PHYSICAL CHEMISTRY Letters

Letter

pubs.acs.org/JPCL

Background-Free Fourth-Order Sum Frequency Generation Spectroscopy

Michael Schleeger,* Maksim Grechko, and Mischa Bonn*

Department of Molecular Spectroscopy, Max Planck Institute for Polymer Research, Ackermannweg 10, 55128 Mainz, Germany

Ⓢ *Supporting Information*

ABSTRACT: The recently developed 2D sum frequency generation spectroscopy offers new possibilities to analyze the structure and structural dynamics of interfaces in a surface-specific manner. Its implementation, however, has so far remained limited to the pump−probe geometry, with its inherent restrictions. Here we present 2D SFG experiments utilizing a novel noncollinear geometry of four incident laser pulses generating a 2D SFG response, analogous to the triangle geometry applied in bulk-sensitive 2D infrared spectroscopy. This approach allows for background-free measurements of fourth-order nonlinear signals, which is demonstrated by measuring the fourth-order material response from a GaAs (110) surface. The implementation of phase-sensitive detection and broadband excitation pulses allows for both highest possible time resolution and high spectral resolution of the pump axis of a measured 2D SFG spectrum. To reduce the noise in our spectra, we employ a referencing procedure, for which we use noncollinear pathways and individual focusing for the signal and local oscillator beams. The 2D spectra recorded from the GaAs (110) surface show nonzero responses for the real and imaginary component, pointing to contributions from resonant electronic pathways to the $\chi^{(4)}$ response.

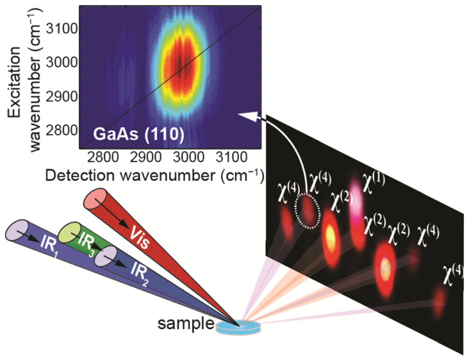

Vibrational sum frequency generation (SFG) spectroscopy provides the unique opportunity to study molecular structures at interfaces. As an optical spectroscopy, SFG has been widely used to investigate a vast variety of liquid and solid interfaces while avoiding any appreciable perturbation of a sample. It has been extensively utilized for characterizing the structures of molecular monolayers of amphiphiles and peptides at liquid and solid interfaces.[1−6] Notably, phase-resolved SFG techniques applied to interfacial water have provided experimental evidence of an averaged orientation of water dipoles according to the charge of amphiphile molecules.[7−10] Further developments of time-resolved and 2D SFG spectroscopies have recently enabled investigations of the vibrational dynamics of molecular monolayers and interfacial water.[8,11−19] Ideally, to characterize interfacial vibrational dynamics without any assumptions, the fourth-order optical susceptibility, $\chi^{(4)}$, would need to be measured.[20] The implementation of such a measurement is challenging because in a typical experimental geometry the $\chi^{(4)}$ optical response is emitted along the same direction as the much stronger second-order ($\chi^{(2)}$) response due to the phase-matching conditions. Thus, upon the detection, multiple signals interfere, which may complicate the interpretation of the measured data. Measuring for instance a superposition of the $\chi^{(2)}$ and $\chi^{(4)}$ sample responses can drastically affect the detected lineshapes.[19] Distorted lineshapes may hinder measurements of waiting time-dynamics of the ellipticity of lines, a measure of spectral diffusion dynamics. The collinearity of $\chi^{(4)}$ and $\chi^{(2)}$ signals stems from the pump−probe geometry utilized in previous implementations, by us and others, of these experiments. In the pump−probe geometry, either single or two collinear pump pulses are used. These techniques are analogous to the conventional bulk pump−probe and collinear 2D spectroscopies, respectively, in which a third-order nonlinear response, $\chi^{(3)}$, is emitted collinear with the linear, $\chi^{(1)}$, signal. From the bulk nonlinear spectroscopy, it is well known that the $\chi^{(3)}$ signal can be measured in a background-free manner when a noncollinear (boxcar or triangle) geometry is used.[21] In a noncollinear geometry, two pump pulses are incident onto a sample from different directions, which imposes a unique direction for the emitted $\chi^{(3)}$ response by the virtue of phase matching. Because similar phase-matching determines the direction of the $\chi^{(4)}$ signal in the SFG spectroscopy, utilization of a noncollinear geometry yields background-free $\chi^{(4)}$ signals.[22]

Here we report an experimental implementation of a noncollinear geometry to measure background-free time- and frequency-resolved $\chi^{(4)}$ signals, which are generated at the surface of a GaAs single crystal, by mixing three broadband mid-infrared and one narrowband upconverting (800 nm) pulses. Details of our experimental setup are given in the Experimental Methods section. In brief, noncollinear infrared pump (IR_1 and IR_2), probe (IR_3), and upconverting (Vis) pulses, with wave vectors $\vec{k}_1$, $\vec{k}_2$, $\vec{k}_3$, and $\vec{k}_{vis}$, respectively, are overlapped in space and time at the focus of a 11 cm concave mirror (Figure 1a). To optimize the beam overlap, we place a

Received: April 13, 2015
Accepted: May 20, 2015
Published: May 20, 2015

DOI: 10.1021/acs.jpclett.5b00768
J. Phys. Chem. Lett. 2015, 6, 2114−2120

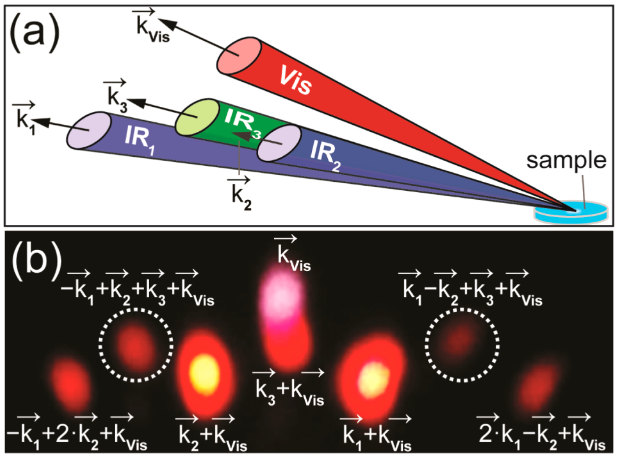

Figure 1. (a) Schematic of the laser beams layout after reflection from a sample surface. (b) SFG signals from a $LiNbO_3$ crystal observed on a paper card. The associated phase-matching directions are indicted by the respective wave vectors. The $\chi^{(4)}$ responses produced by mixing of all four laser pulses are indicated by dotted circles.

horizontally oriented 1 mm thick lithium niobate ($LiNbO_3$) crystal into the focus of the mirror and monitor the emerging SFG signals. Overlaps of IR$_1$, IR$_2$, and IR$_3$ with Vis in the bulk of the crystal produce three $\chi^{(2)}$ SFG signals in the $\vec{k}_1 + \vec{k}_{vis}$, $\vec{k}_2 + \vec{k}_{vis}$, and $\vec{k}_3 + \vec{k}_{vis}$ phase-matching directions, respectively. A fraction of these signals is reflected from the bottom surface of the crystal. Because of the bulk origin of the signals and the high optical nonlinearity of $LiNbO_3$, these reflected pulses can be readily observed with the naked eye on a paper card (Figure 1b). By maximizing the $\chi^{(2)}$ signals we individually optimize the spatial and temporal overlap for each mid-IR pulse with the Vis pulse. Alongside the second order signals, mixing of the pulses produces intense fourth-order responses, which are also observed on a paper card. $\chi^{(4)}$ signals generated by the mixing of all *four* pulses are emitted in the $-\vec{k}_1 + \vec{k}_2 + \vec{k}_3 + \vec{k}_{vis}$ and $\vec{k}_1 - \vec{k}_2 + \vec{k}_3 + \vec{k}_{vis}$ directions.[21] We note that in the $-\vec{k}_1 + 2\vec{k}_2 + \vec{k}_{vis}$ and $2\vec{k}_1 - \vec{k}_2 + \vec{k}_{vis}$ directions we also observe $\chi^{(4)}$ signals generated by mixing of only three pulses, which are not of our primary interest. By monitoring intensities of the $\chi^{(4)}$ signals we optimize time and space overlap of all four incident pulses.

SFG signals produced by the $LiNbO_3$ crystal are essentially bulk signals. To demonstrate feasibility of our approach for the surface science, we measure the $\chi^{(4)}$ optical response from the (110) surface of a GaAs single crystal. Because the surface nonlinear optical responses are much weaker than the bulk responses, for example, not observable by eye, it is demanding to align them to the detector. Thus, to set up the beam path to the detector for the $\chi^{(4)}$ response in the reflection geometry, we use the intense $\chi^{(4)}$ signal produced in $LiNbO_3$. For this purpose, we place a $LiNbO_3$ crystal and GaAs wafer on two manual goniometers. Both goniometers are mounted on a vertical translation stage, which, in turn, is installed on a horizontal translation stage. Utilization of the vertical and horizontal translation stages allows a fast and easy exchange of the sample at the focus of the laser beams. We orient $LiNbO_3$ and GaAs surfaces parallel to each other by monitoring the reflection of an auxiliary continuous-wave (CW) laser beam. Next, we align the $\chi^{(4)}$ signal reflected from the bottom surface of the $LiNbO_3$ crystal to the spectrometer. Because the $LiNbO_3$ and GaAs surfaces are parallel, the $\chi^{(4)}$ signal from the GaAs follows the path of that from the $LiNbO_3$ when we exchange the sample, and no additional manipulations are necessary.

The $\chi^{(4)}$ signal from the sample is focused on the entrance slit of the spectrometer by a spherical lens and detected by a charge-coupled device (CCD) camera. Figure 2a shows the $\chi^{(4)}$ spectrum generated at the (110) GaAs surface in the $-\vec{k}_1 + \vec{k}_2 + \vec{k}_3 + \vec{k}_{vis}$ direction when all of the laser pulses are p-polarized (for a spectrum with longer acquisition time see Supporting Information). The line width of this spectrum is determined by the bandwidth of the probe infrared pulse (IR$_3$), as the response of the GaAs is spectrally very broad. The intensity of the $\chi^{(4)}$ response depends on the time delays between the laser pulses. Initially, all the pulses are overlapped in time, which produces the maximum signal. With increasing time delay t_1 between the IR$_1$ and IR$_2$ pulses (Figure 2b), the intensity of the signal decreases (Figure 2c,d). Because of the spectrally broad GaAs $\chi^{(4)}$ signal, we believe that the signal decay in Figure 2c,d is mainly determined by the time overlap of the laser pulses. As it is detected in the $-\vec{k}_1 + \vec{k}_2 + \vec{k}_3 + \vec{k}_{vis}$ direction, the signal in Figure 2 is analogous to the conventional bulk photon echo (rephasing) signal.[23]

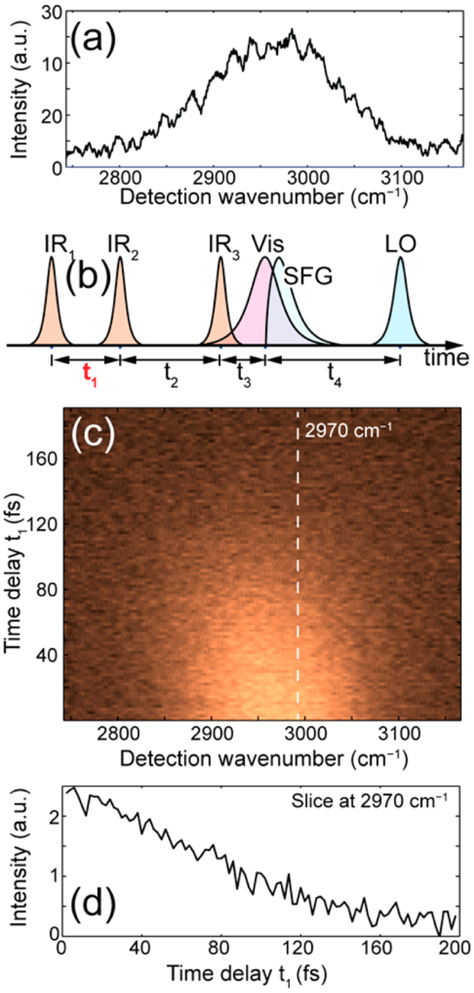

Figure 2. (a) Homodyne-detected $\chi^{(4)}$ signal from GaAs (110) surface produced at zero time delay between the laser pulses (i.e., $t_1 = t_2 = t_3 = 0$; no local oscillator LO). (b) Sequence of the laser pulses used in the experiment. The time delays between the pulses are denoted by t_1, t_2, t_3, and t_4. (c) The signal from panel a at different t_1 time delays, for $t_2 = t_3 = 0$. (d) A slice of the plot in panel c along the dashed line.

The homodyne detection of the $\chi^{(4)}$ signal in Figure 2 is easy to implement, but it has significant drawbacks. First, it lacks phase information, which is needed for determining up and down orientations of molecules at an interface.[7−10] Second, the homodyne detection can be used to correlate pump-and-probe frequencies only when a narrowband pump pulse is employed. Such a correlation is essential for revealing molecular vibrational dynamics and, for the homodyne detection, is done by measuring the $\chi^{(4)}$ spectrum when pumping at a given pump frequency. Thus, when applying homodyne detection, a narrowband pump pulse is needed to unambiguously determine the pump frequency. Narrowing of the pump spectrum increases spectral resolution along the pump frequency axis, but at the same time it decreases time resolution of the experiment due to the longer pump pulse. It has been previously demonstrated that both of these drawbacks can be overcome by using heterodyne detection.[8,18,24] For the heterodyne detection, an additional local oscillator (LO) pulse is employed. The LO pulse is overlapped with the signal at the detector to produce interference. Because the interference term is proportional to the electric field of the signal, rather than its intensity, it contains the phase information on the signal field. Furthermore, the phase of the interference is proportional to the time delay t_1 and the pump frequency. Accordingly, the pump frequency axis can be reconstructed by measuring the interference at different t_1 time delays and performing the Fourier transform. Because of the use of broadband, and thus short, pump pulses, the heterodyne detection approach provides the best possible time resolution. The frequency resolution along the pump axis is then determined by the longest t_1 time delay in the scan and can achieve subwavenumber, employing common delay stages and spectrometers.

For the implementation of the heterodyne detection, we produce the LO by SFG in a different $LiNbO_3$ crystal. For this, we refocus the IR_3 and Vis pulses reflected from the samples (see Experimental Methods for details). Thus, the LO propagates noncollinear to the fourth-order signal generated by the sample. Before the spectrometer, we align the signal and the LO in the vertical plane so that they come to the same position at the entrance slit of the spectrometer. We use a cylindrical lens to focus the LO onto the spectrometer slit, which simplifies spatial overlapping of the LO and signal as well as enables referencing, as explained below. Because the spectrometer creates a frequency dispersed image of the entrance slit on the chip of the CCD camera, the interference pattern of the LO and $\chi^{(4)}$ signal at the slit is mapped onto the camera (Figure 3a,b). Because the $\chi^{(4)}$ signal is tightly focused by a spherical lens, its image on the camera is only a few pixels in height. In contrast, the LO is detected across all rows of the image because it is focused by the cylindrical lens. In the area of the CCD chip where the two signals overlap, clear interference fringes are observed. The fringes are out-of-phase at the adjacent rows, likely due to the nonzero angle in the vertical plane between the $\chi^{(4)}$ signal and LO incident onto the entrance slit of the spectrometer.

The signal row in Figure 3b contains three contributions: the intensity of the LO, of the $\chi^{(4)}$, and an interference term Signal $= |E_{LO}|^2 + |E_{\chi(4)}|^2 + 2E_{LO}E_{\chi(4)}$.[7,10] The first two terms do not have any phase information, and they are readily subtracted from the data (see Experimental Methods for details). Figure 4a shows interference fringes at the signal row after the subtraction. Because the phase of the $\chi^{(4)}$ is proportional to the time delay t_1 between the two pump pulses, the interference pattern changes in an oscillating manner when t_1 is scanned (Figure 4b,c). By Fourier transform of the scan in Figure 4b we obtain 2D SFG spectrum for the (110) surface of the GaAs (Figure 4d). As we can see, the 2D spectrum has significant distortions because of the noise in the time-domain scan (Figure 4b,c). The noise in the time-domain scan originates mainly from the background fluctuations due to the intensity fluctuations of the LO pulse, which were not eliminated by the background subtraction previously described. To improve the signal-to-noise ratio in our spectra we use referencing. For this, we subtract the reference row from the signal row in Figure 3b for each t_1 step. This allows us to eliminate the LO intensity term. In particular, referencing completely eliminates background fluctuations and significantly improves signal-to-noise ratio in the 2D spectrum (Figure 4e−h). We note that the referencing in our setup is possible due to utilization of different focusing lenses, spherical and cylindrical, for the signal and LO, respectively. This approach enables independent measurement of the LO intensity for each t_1 step using a single CCD camera. Note that the waiting time, t_2, during which spectral diffusion takes place, is set close to zero in our experiment.

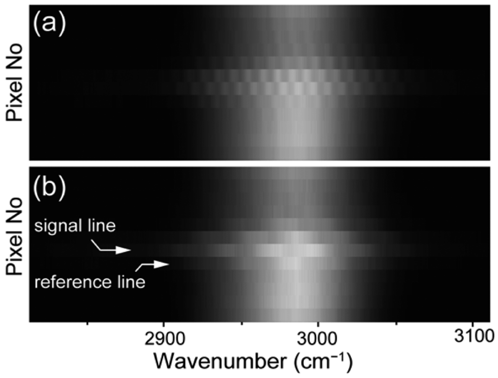

Figure 3. Detected signal image from a GaAs (110) single crystal surface with the vertically broad LO signal filling the full vertical space of the presented CCD camera area and the focused $\chi^{(4)}$ signal spanning 4 pixels. An interference pattern is detected within the overlapping region of LO and $\chi^{(4)}$ signal. In panel a a high periodicity of the interference fringes is observed, corresponding to a larger time difference between LO and $\chi^{(4)}$ signal across the frequency axis, experimentally controlled by a wedge pair. In panel b a smaller time delay was selected, corresponding to the separation in the following experiments. Note the difference between vertical and horizontal scales: the vertical scale is 12 pixels; the horizontal scale is 390 pixels.

The absolute value spectra in Figure 4d,h do not contain any phase information, which is needed to determine up and down molecular orientations and distinguish fundamental and sequential transitions. To obtain this information, we need the real and imaginary parts of the $\chi^{(4)}$ spectrum. The calculation of real and imaginary spectra from the measured response requires precise knowledge of the phasing, which depends on the precise values (i.e., determined with subcycle precision) for zero time delays for t_1 and t_4. A rough estimate for $t_1 = 0$ is deduced from the maximum of the signal in the homodyne scan (Figure 2c,d). In the heterodyne scan (Figure 4), for zero t_1 and t_4 the interference phase between the $\chi^{(4)}$ signal and the LO is uniform for all wavelengths. We use this criterion alongside the derived $t_1 = 0$ for a rough determination of the $t_4 = 0$. For a purely nonresonant response, a further

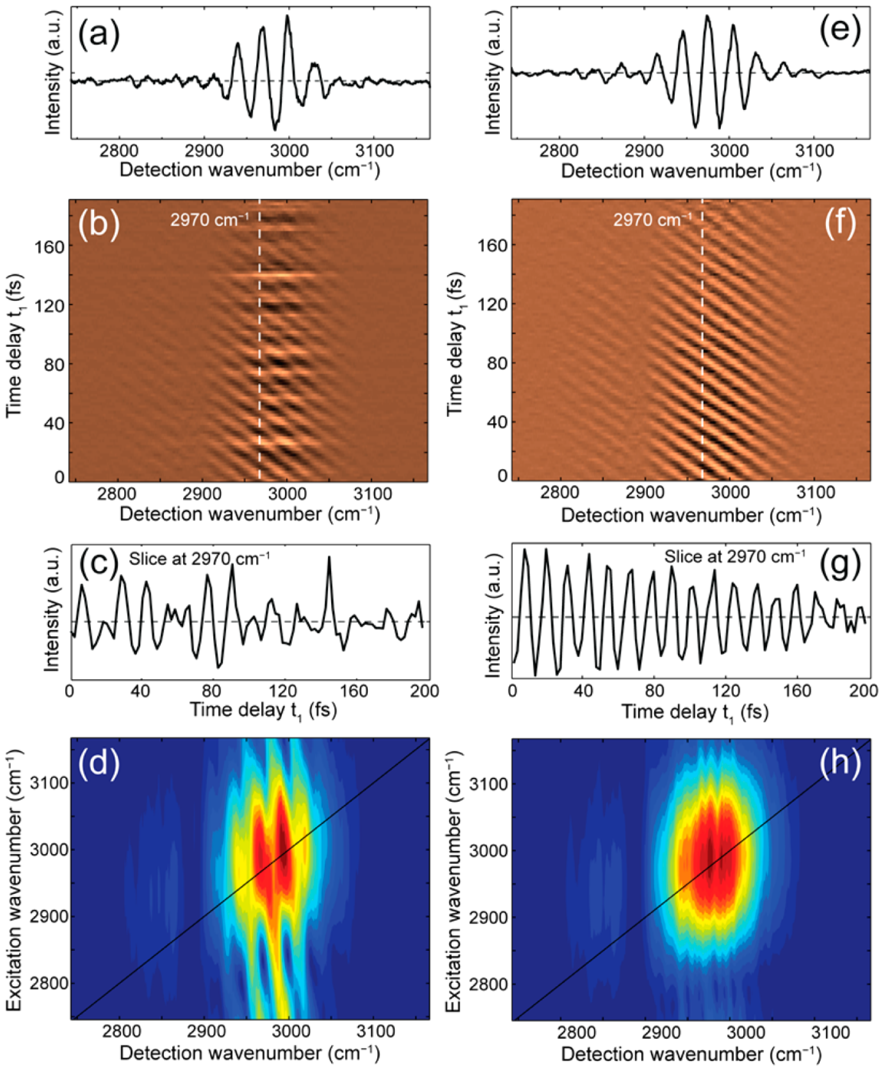

Figure 4. Left side figures (a−d) are constructed by data based on a single row from the detector camera; the right side employs additional subtraction of a reference row and thus suppresses noise arising from laser intensity fluctuations. (a,e) Heterodyned echo $\chi^{(4)}$ spectra of GaAs (110) at maximal time overlap of all incident laser pulses. (b,f) Interference of the $\chi^{(4)}$ and LO as a function of the t_1. The dashed white lines indicate the positions of the slices (2970 cm^{-1}) plotted in panels c and g. (d,h) Absolute value 2D SFG spectra, obtained by Fourier transform of the data in panels b and f, respectively.

criterion for an accurate phasing is the vanishing of the imaginary part of the optical response.[8] Using our data set, it was not possible to find such phase corrections,[25] for which the real or the imaginary part of the $\chi^{(4)}$ vanishes. This indicates that the measured signal stems from resonant excitation pathways. Indeed, because the GaAs sample we used was kept in the air during the experiments its surface is terminated with an oxide layer.[26] This may result in the presence of shallow donor states that can be depopulated by the 3 μm infrared pulses, giving rise to a large interfacial polarization. Moreover, free carriers will be generated in the near-surface region before the IR pulses by the long, ~1 ps, Vis pulse, which excites the interband transition (the 800 nm photon energy, 1.55 eV, exceeds the GaAs bandgap energy). It is likely that the generated free carriers also contribute to the interfacial polarization. Assuming the resonant nature of the measured $\chi^{(4)}$ response, we propose the phasing that yields absorptive and dispersive line shapes for the imaginary and real component of the $\chi^{(4)}$ spectra, respectively. Note that a 90° phase shift swaps real and imaginary spectra, whereas a 180° phase shift results in alternated signs of the spectral responses. Figure 5a,b shows the real and imaginary 2D SFG echo spectra with a negative and positive peak pair and a negative peak, respectively. The elongation along the diagonal of the 2D peaks in Figure 5a,b can be attributed to a noninstantaneous spectral diffusion, slower than the experimental time resolution.

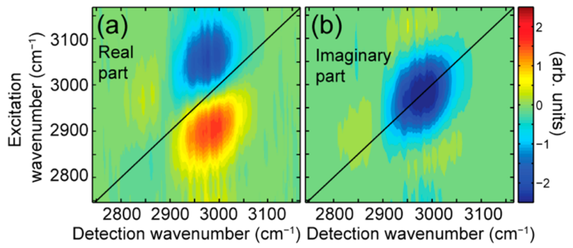

Figure 5. Phase-corrected real (a) and imaginary (b) echo 2D SFG spectra of GaAs (110).

DOI: 10.1021/acs.jpclett.5b00768
J. Phys. Chem. Lett. 2015, 6, 2114−2120

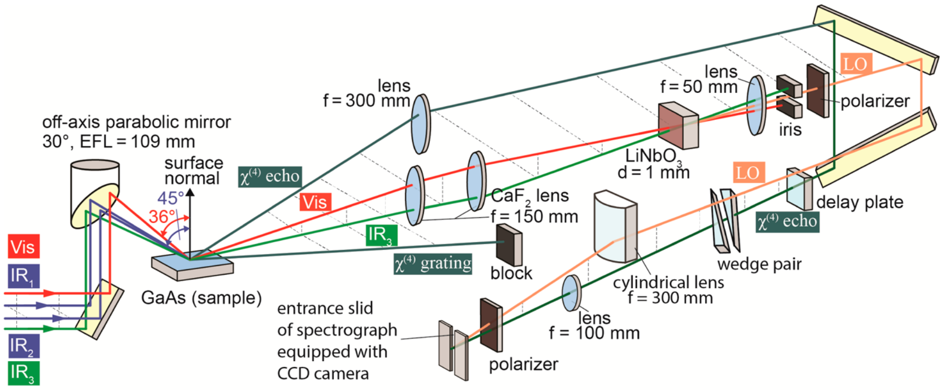

Figure 6. Optical layout of the sample and detection compartment of the time domain $\chi^{(4)}$ experiment in noncollinear geometry. For the sake of clarity, the IR$_1$ and IR$_2$ beams reflected from the sample as well as the various nonlinear responses are not shown.

The proposed phasing procedure is based on the assumption of a resonant nature of the $\chi^{(4)}$ response. However, different resonant pathways previously discussed can have different phases. Moreover, nonresonant pathways and different sequences of light−matter interactions can also contribute to the $\chi^{(4)}$ signal. Thus, the phasing of the measured spectra is still arguable. In addition, a deviation from the (semi-) impulsive limit, for which the laser pulses are much shorter than the material response, may distort the derived line shapes. We believe that rigorous phasing may be achieved by measuring the fully nonresonant $\chi^{(4)}$ response from, for instance, single-crystalline quartz.[7,23] Further experiments to resolve this issue are on the way in our lab.

In conclusion, we demonstrate the successful application of noncollinear 2D SFG spectroscopy for the first time. The noncollinear geometry enabled us to spatially separate the $\chi^{(4)}$ response from a GaAs (110) crystal surface from lower-order signals, providing a background-free fourth-order signal. The heterodyning of the $\chi^{(4)}$ response and scanning of the time delay between an IR pulse pair allowed measurements of 2D SFG spectra in the time-domain. The proposed phased real and imaginary spectra of GaAs (110) suggest a resonant nature of pathways to the $\chi^{(4)}$ response. The noncollinear 2D SFG spectroscopy provides background-free insight into the electronic structure and dynamics of a surface. In the future, we also plan to utilize this technique to investigate molecular structure of interfaces by probing molecular vibrations.

■ EXPERIMENTAL METHODS

The optical layout of the experiment is shown in Figure 6 and in the Supporting Information (SI). The fundamental light of a Ti:sapphire regenerative amplifier (Legend Elite F-HE, Coherent, 4.3 mJ, centered at 800 nm, 100 fs pulse duration, and 1 kHz repetition rate) was split into four beams. Two intense broadband IR pulses (IR$_1$ and IR$_2$ in Figure S1, SI) were generated in a multistep procedure: A home-built optical parametric amplifier (OPA, similar to ref 27) was pumped with ~1 mJ of 800 nm light. The second harmonic (~1050 nm) of the OPA output idler pulse was generated in a barium borate crystal (β-BBO). This second harmonic pulse was mixed with 1 mJ, 800 nm pulse in a potassium titanyl phosphate (KTP) crystal for the difference frequency generation (DFG). The DFG produced a mid-IR pulse centered at ~3390 nm (2950 cm^{-1}), with ~70 μJ energy, ~100 fs pulse duration, and a bandwidth of 160 cm^{-1} (fwhm). This mid-IR pulse was split by a 50% beamsplitter to produce the two pump pulses (IR$_1$ and IR$_2$). We use motorized translation stages (M-405-DG, Physik Instrumente (PI), Karlsruhe, Germany) to control time delays of the IR$_1$ and IR$_2$. A third broadband IR pulse (IR$_3$) was generated by 1 mJ of 800 nm radiation using a commercial OPA (TOPAS equipped with a noncollinear difference frequency generator, DFG, with tuning range in the infrared from 2.6 to 11 μm, Light Conversion). The energy of the IR$_3$ is ~5 μJ and the frequency of the TOPAS was tuned to match the frequencies of the pump pulses. A fourth beam of 800 nm radiation (Vis) was passed through a 4-f pulse shaper, which reduces the pulse bandwidth to ~20 cm^{-1}, and attenuated to ~850 nJ and used for upconversion.

The IR$_{1-3}$ and Vis pulses were focused onto a sample by a parabolic mirror (30° off-axis, effective focal length EFL = 109 mm). Angles of incidence were 36 and 45° for the Vis and IR$_3$ beams, respectively; the IR$_1$ and IR$_2$ beams both had incident angles of 43° in the vertical plane and diverged by +12° (IR$_2$) and −12° (IR$_1$) in the horizontal plane. The reflected IR$_3$ and Vis beams were collimated and focused into a LiNbO$_3$ crystal (thickness: 1 mm) by a CaF$_2$ lens pair to generate a local oscillator (LO) pulse by bulk SFG. The transmitted LO was collimated, passed through a first linear polarizer (extinction ratio ~10^6), and focused onto the entrance slit of a spectrometer (Acton SP2300) by a cylindrical lens. Because the LO is generated by reflections of the Vis and IR$_3$ pulses, both reflections from the top and bottom surfaces of the crystal can produce LO pulses. Such LO pulses have similar intensities but significantly different time delays (~10 ps) at the detector. To select one of them, we coated the bottom surface of the LiNbO$_3$ crystal by a silver film. The $\chi^{(4)}$ echo signal beam was collimated by a lens (f = 300 mm). To match the time delay of the LO, the time delay of the $\chi^{(4)}$ signal was increased by a fused silica window (5 mm, with antireflection coating) and fine-tuned by a wedge pair (fused silica, 50 × 25 × 2 mm (center), 4° wedge, Venteon, Hannover, Germany). The signal was focused by a plano-convex spherical lens (f = 100 mm) onto the spectrometer entrance slit and overlapped with the LO pulse. To control polarizations of the detected beams, we installed a second linear polarizer in front of the spectrometer. The spectrally dispersed signal was measured by CCD camera (Andor iXon+).

For acquiring time-domain 2D SFG spectra from a GaAs (110) crystal surface, a single time scan from −200 to 200 fs in 2 fs steps was performed with 10 s accumulation time per delay position for the homodyne data and 100 s accumulation for the heterodyne data set. A zero-padding by a factor 100 was applied

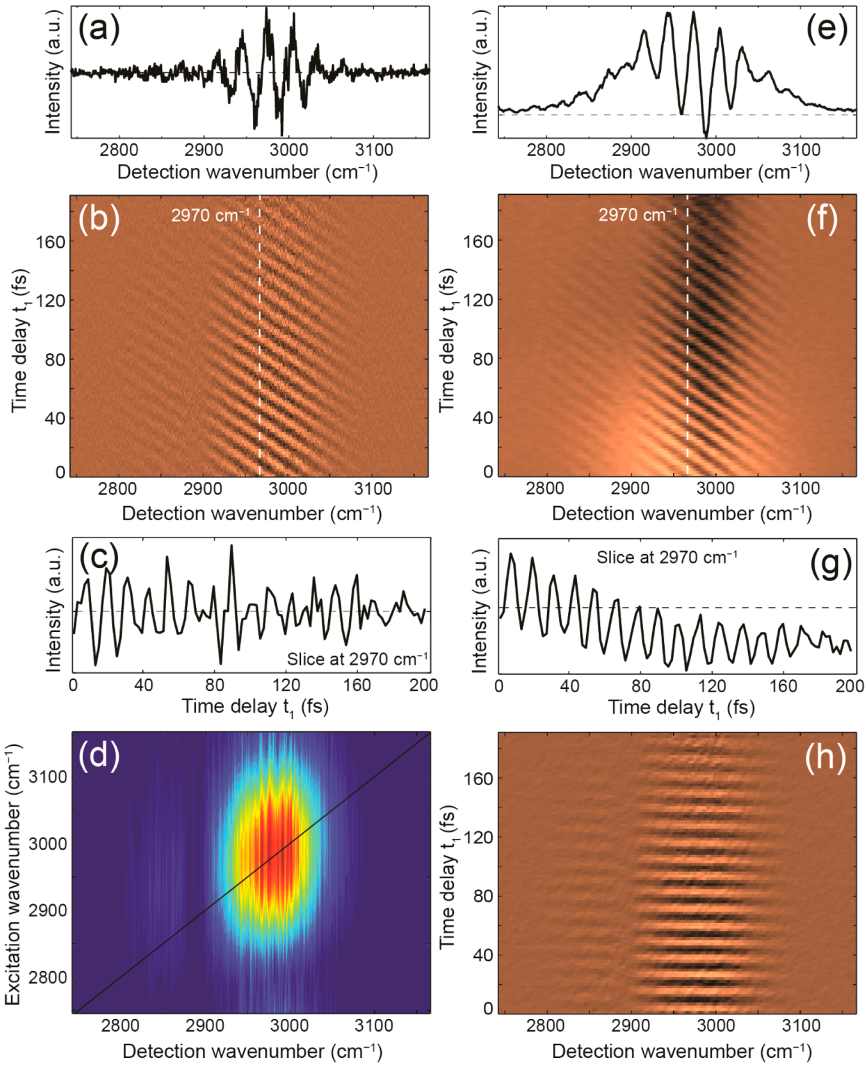

Figure 7. Interferences and 2D $\chi^{(4)}$ plots analogous to Figure 4. (a−g) Examples of different data processing, which involves subtraction of a reference together with subtraction of the homodyne $\chi^{(4)}$ contribution (for panels b−d) or smoothing along the detection wavenumber axis (for panels e−g). (h) Data of Figure 4f are plotted after performing the phase correction. The interference pattern for small time delays t_1 is aligned parallel to the detection wavenumber axis, indicating a uniform phase between the $\chi^{(4)}$ signal and LO for all wavelengths.

prior to the Fourier transform. The spectral resolution of the measured detection wavenumber axis (0.0535 nm or 1.27 cm^{-1}) strongly exceeds the spectral width of the upconverting 800 nm pulse (∼0.84 nm or ∼20 cm^{-1}). Therefore, a smoothing procedure was applied to additionally decrease the noise level by calculating the mean value of neighboring 10 data points. Examples of different data processing are shown in Figure 7a−d.

■ ASSOCIATED CONTENT

Ⓢ Supporting Information

Further details on the optical layout of the employed setup. The Supporting Information is available free of charge on the ACS Publications website at DOI: 10.1021/acs.jpclett.5b00768.

■ AUTHOR INFORMATION

Corresponding Authors

*E-mail: schleeger@mpip-mainz.mpg.de.
*E-mail: bonn@mpip-mainz.mpg.de.

Notes

The authors declare no competing financial interest.

■ ACKNOWLEDGMENTS

This work is supported by NanoNextNL, a micro and nanotechnology consortium of the Government of The Netherlands and 130 partners. We are grateful to Dr. Victor Volkov for initiating this project, the initial construction of the experimental setup, and for guidance and support during the further development of the setup.

■ REFERENCES

(1) Zhuang, X.; Miranda, P. B.; Kim, D.; Shen, Y. R. Mapping Molecular Orientation and Conformation at Interfaces by Surface Nonlinear Optics. *Phys. Rev. B* **1999**, *59*, 12632−12640.

(2) Miranda, P. B.; Shen, Y. R. Liquid Interfaces: A Study by Sum-Frequency Vibrational Spectroscopy. *J. Phys. Chem. B* **1999**, *103*, 3292−3307.

(3) Chen, Z.; Shen, Y. R.; Somorjai, G. A. Studies of Polymer Surfaces by Sum Frequency Generation Vibrational Spectroscopy. *Annu. Rev. Phys. Chem.* **2002**, *53*, 437−465.

(4) Messmer, M. C.; Conboy, J. C.; Richmond, G. L. Observation of Molecular Ordering at the Liquid-Liquid Interface by Resonant Sum-Frequency Generation. *J. Am. Chem. Soc.* **1995**, *117*, 8039−8040.

(5) Raymond, E. A.; Richmond, G. L. Probing the Molecular Structure and Bonding of the Surface of Aqueous Salt Solutions. *J. Phys. Chem. B* **2004**, *108*, 5051−5059.

(6) Fu, L.; Ma, G.; Yan, E. C. Y. In Situ Misfolding of Human Islet Amyloid Polypeptide at Interfaces Probed by Vibrational Sum Frequency Generation. *J. Am. Chem. Soc.* **2010**, *132*, 5405−5412.

(7) Nihonyanagi, S.; Yamaguchi, S.; Tahara, T. Direct Evidence for Orientational Flip-Flop of Water Molecules at Charged Interfaces: a Heterodyne-Detected Vibrational Sum Frequency Generation Study. *J. Chem. Phys.* **2009**, *130*, 204704.

(8) Singh, P. C.; Nihonyanagi, S.; Yamaguchi, S.; Tahara, T. Ultrafast Vibrational Dynamics of Water at a Charged Interface Revealed by Two-Dimensional Heterodyne-Detected Vibrational Sum Frequency Generation. *J. Chem. Phys.* **2012**, *137*, 94706.

(9) Chen, X.; Hua, W.; Huang, Z.; Allen, H. C. Interfacial Water Structure Associated with Phospholipid Membranes Studied by Phase-Sensitive Vibrational Sum Frequency Generation Spectroscopy. *J. Am. Chem. Soc.* **2010**, *132*, 11336−11342.

(10) Pool, R. E.; Versluis, J.; Backus, E. H.; Bonn, M. Comparative Study of Direct and Phase-Specific Vibrational Sum-Frequency Generation Spectroscopy: Advantages and Limitations. *J. Phys. Chem. B* **2011**, *115*, 15362−15369.

(11) McGuire, J. A.; Shen, Y. R. Ultrafast Vibrational Dynamics at Water Interfaces. *Science* **2006**, *313*, 1945−1948.

(12) Smits, M.; Ghosh, A.; Sterrer, M.; Muller, M.; Bonn, M. Ultrafast Vibrational Energy Transfer between Surface and Bulk Water at the Air-Water Interface. *Phys. Rev. Lett.* **2007**, *98*, 98302.

(13) Ghosh, A.; Smits, M.; Bredenbeck, J.; Bonn, M. Membrane-Bound Water is Energetically Decoupled from Nearby Bulk Water: An Ultrafast Surface-Specific Investigation. *J. Am. Chem. Soc.* **2007**, *129*, 9608−9609.

(14) Bonn, M.; Bakker, H. J.; Ghosh, A.; Yamamoto, S.; Sovago, M.; Campen, R. K. Structural Inhomogeneity of Interfacial Water at Lipid Monolayers Revealed by Surface-Specific Vibrational Pump-Probe Spectroscopy. *J. Am. Chem. Soc.* **2010**, *132*, 14971−14978.

(15) Nihonyanagi, S.; Singh, P. C.; Yamaguchi, S.; Tahara, T. Ultrafast Vibrational Dynamics of a Charged Aqueous Interface by Femtosecond Time-Resolved Heterodyne-Detected Vibrational Sum Frequency Generation. *Bull. Chem. Soc. Jpn.* **2012**, *85*, 758−760.

(16) Zhang, Z.; Piatkowski, L.; Bakker, H. J.; Bonn, M. Ultrafast Vibrational Energy Transfer at the Water/Air Interface Revealed by Two-Dimensional Surface Vibrational Spectroscopy. *Nat. Chem.* **2011**, *3*, 888−893.

(17) Zhang, Z.; Piatkowski, L.; Bakker, H. J.; Bonn, M. Communication: Interfacial Water Structure Revealed by Ultrafast Two-Dimensional Surface Vibrational Spectroscopy. *J. Chem. Phys.* **2011**, *135*, 21101.

(18) Laaser, J. E.; Skoff, D. R.; Ho, J. J.; Joo, Y.; Serrano, A. L.; Steinkruger, J. D.; Gopalan, P.; Gellman, S. H.; Zanni, M. T. Two-Dimensional Sum-Frequency Generation Reveals Structure and Dynamics of a Surface-Bound Peptide. *J. Am. Chem. Soc.* **2014**, *136*, 956−962.

(19) Xiong, W.; Laaser, J. E.; Mehlenbacher, R. D.; Zanni, M. T. Adding a Dimension to the Infrared Spectra of Interfaces Using Heterodyne Detected 2D Sum-Frequency Generation (HD 2D SFG) Spectroscopy. *Proc. Nat. Acad. Sci. U. S. A.* **2011**, *108*, 20902−20907.

(20) Gengeliczki, Z.; Rosenfeld, D. E.; Fayer, M. D. Theory of Interfacial Orientational Relaxation Spectroscopic Observables. *J. Chem. Phys.* **2010**, *132*, 244703.

(21) Fecko, C. J.; Eaves, J. D.; Loparo, J. J.; Tokmakoff, A.; Geissler, P. L. Ultrafast Hydrogen-Bond Dynamics in the Infrared Spectroscopy of Water. *Science* **2003**, *301*, 1698−702.

(22) Volkov, V. Sum-Frequency Generation Echo and Grating from Interface. *J. Chem. Phys.* **2014**, *141*, 144103.

(23) Ge, N. H.; Zanni, M. T.; Hochstrasser, R. M. Effects of Vibrational Frequency Correlations on Two-Dimensional Infrared Spectra. *J. Phys. Chem. A* **2002**, *106*, 962−972.

(24) Hsieh, C. S.; Okuno, M.; Hunger, J.; Backus, E. H. G.; Nagata, Y.; Bonn, M. Aqueous Heterogeneity at the Air/Water Interface Revealed by 2D-HD-SFG Spectroscopy. *Angew. Chem., Int. Ed.* **2014**, *53*, 8146−8149.

(25) Asbury, J. B.; Steinel, T.; Fayer, M. D. Vibrational Echo Correlation Spectroscopy Probes of Hydrogen Bond Dynamics in Water and Methanol. *J. Lumin.* **2004**, *107*, 271−286.

(26) Barton, J. J.; Goddard, W. A.; Mcgill, T. C. Reconstruction and Oxidation of the GaAs(110) Surface. *J. Vac. Sci. Technol.* **1979**, *16*, 1178−1185.

(27) Hamm, P.; Kaindl, R. A.; Stenger, J. Noise Suppression in Femtosecond Mid-Infrared Light Sources. *Opt. Lett.* **2000**, *25*, 1798−1800.